Enhanced Photocatalytic Reduction of Methyl Viologen by Self-Assembling Ruthenium(II)Poly(Pyridyl) Complexes with L-Lysine Containing Side Chains

Masahiro Suzuki, Chad C. Waraksa, Thomas E. Mallouk,* Hiroko Nakayama,† and Kenji Hanabusa†

Department of Chemistry, The Pennsylvania State University, University Park, Pennsylvania 16802

Received: November 2, 2001; In Final Form: January 24, 2002

New tris(2,2′-bipyridine)-type ruthenium(II) complexes with L-lysine-containing side chains form gels by hierarchical assembly of hydrogen bonded fibers in some organic solvents. These Ru(II) complex aggregates are more efficient photosensitizers for reduction of methyl viologen than $Ru(bpy)_3^{2+}$ in the presence of triethanolamine, a sacrificial electron donor. The increased rate of reduced viologen formation arises from an increased charge separation lifetime and an increased rate of reduction of Ru(III) to Ru(II) by triethanolamine.

Introduction

Self-assembly is one of the most useful tools available to chemists for organizing complex photoredox systems for vectorial electron transfer. In the broadest definition, self-assembly refers to a process by which a structurally well-defined supramolecular aggregate forms spontaneously from its component molecules. Well-known examples include monolayer assembly, membrane formation, molecular recognition (i.e., substrate binding to proteins, DNA/protein interactions, antibody/antigen interactions), metal ion coordination, and fiber and network assemblies.[1−3] These structures are held together by relatively weak intermolecular forces which include hydrogen bonding, π-stacking, van der Waals interactions, hydrophobic/hydrophilic interactions, ionic forces, and relatively labile metal−ligand coordination interactions. Often, these materials are characterized by hierarchical structures, i.e., by organization on more than one length scale. Many low molecular weight compounds that form a hierarchical network of superstructures in organic fluids have now been synthesized[3−5] and have been applied to the fabrication of templated materials,[6,7] sensors,[8] and assemblies with molecular recognition and other useful properties.[9,10]

Recently, we have reported the supramolecular structure of L-lysine derivatives that form nanometer-scale fibers in various organic fluids.[11] These compounds create a hierarchical network by entangling of fibers, and they can gel many organic solvents. More recently, an L-lysine viologen derivative, which forms fibrous aggregates in some aromatic solvents, has been synthesized, and its photosensitized charge separation reaction has been investigated using $Ru(bpy)_3^{2+}$ as a photosensitizer.[12] The initial rate of viologen radical formation for this self-assembling system is higher than that for methyl viologen (MV^{2+}) in the analogous homogeneous system. Here, we describe the synthesis of new ruthenium(II)poly(pyridyl) complexes with L-lysine containing side chains. These photosensitizers form nanometer scale fibrous assemblies, and show enhanced quantum yields for MV^{2+} photoreduction in methanol-toluene (1:1 v/v), in the presence of the sacrificial donor triethanolamine (TEOA), relative to $Ru(bpy)_3^{2+}$ in the same system.

Experimental Section

Materials. N-ϵ-Lauroyl-L-lysine was supplied from Ajinomoto Co., Inc. All other starting materials were purchased from chemical suppliers and used without further purification. 4,4′-Dimethyl-2,2′-bipyridine,[11] 4,4′-dicarboxy-2,2′-bipyridine,[11] 4,4′-bis(chlorocarbony)-2,2′-bipyridine,[11] and N-ϵ-lauroyl-L-lysine ethyl ester (C_2AmiNH_2)[9] were synthesized according to literature procedures.

Synthesis of 2,2′-Bipyridine Ligand with N-ϵ-Lauroyl-L-lysine Ethyl Esters [$(C_2Ami)_2$bpy]. C_2AmiNH_2 was dissolved in a dry THF solution containing NEt_3, and a dry THF solution of 4,4′-bis(chlorocarbonyl)-2,2′-bipyridine was slowly added in an ice-bath with stirring. The resulting solution was stirred at room temperature for 24 h. The white precipitate was filtered and washed with THF. The mixture of the filtrate and washings was evaporated to dryness. The crude product was dissolved in hot methanol, and the hot solution was quickly filtered. The pure white product was obtained by cooling in a refrigerator for 6 h. Elemental Anal. Calcd. for $C_{52}H_{84}N_6O_8$: C, 67.78; H, 9.21; N, 9.12. Found: C, 67.89; H, 9.22; N, 9.29. Yield 91%.

Synthesis of Ruthenium(II) Complexes. Tris[(C_2Ami_2)bpy]-ruthenium(II) chloride hexahydrate $Ru[(C_2Ami_2)bpy]_3Cl_2\cdot 6H_2O$ (**Ru1**). $RuCl_3\cdot 3H_2O$ and $[(C_2Ami_2)bpy]$ were refluxed in ethanol for 5 d. The hot solution was filtered and evaporated to dryness. The crude solid was dissolved in toluene and filtered. The filtrate was evaporated to dryness. Elemental Anal. Calcd. for $C_{156}H_{264}N_{18}O_{24}Cl_2Ru$: C, 61.55; H, 8.76; N, 8.27. Found: C, 61.88; H, 8.92; N, 8.12. Yield 88%.

$Ru[(C_2Ami)_2bpy][bpy]_2Cl_2\cdot 6H_2O$ (**Ru2**)·$Ru(bpy)_2Cl_2\cdot 2H_2O$ and $(C_2Ami)_2$bpy were refluxed in 80% ethanol for 2 d under an argon atmosphere. The solution was evaporated to dryness. The crude solid was dissolved in a cold acetone, and the insoluble compound was filtered off. The $Ru[C_2Ami)_2bpy][bpy]_2Cl_2\cdot 6H_2O$ was obtained by evaporation of the filtrate to dryness. Elemental Anal. Calcd. for $C_{72}H_{112}N_{10}O_{14}Cl_2Ru$: C, 57.12; H, 7.47; N, 9.25. Found: C, 57.34; H, 7.62; N, 9.33. Yield 92%.

Measurements. Elemental analyses were performed with a Perkin-Elmer series II CHNS/O analyzer 2400. FTIR spectra

* To whom correspondence should be addressed.
† Graduate School of Science and Technology, Shinshu University, Ueda, Nagano 386-8567, Japan.

10.1021/jp014050h CCC: $22.00
Published on Web 03/30/2002

SCHEME 1

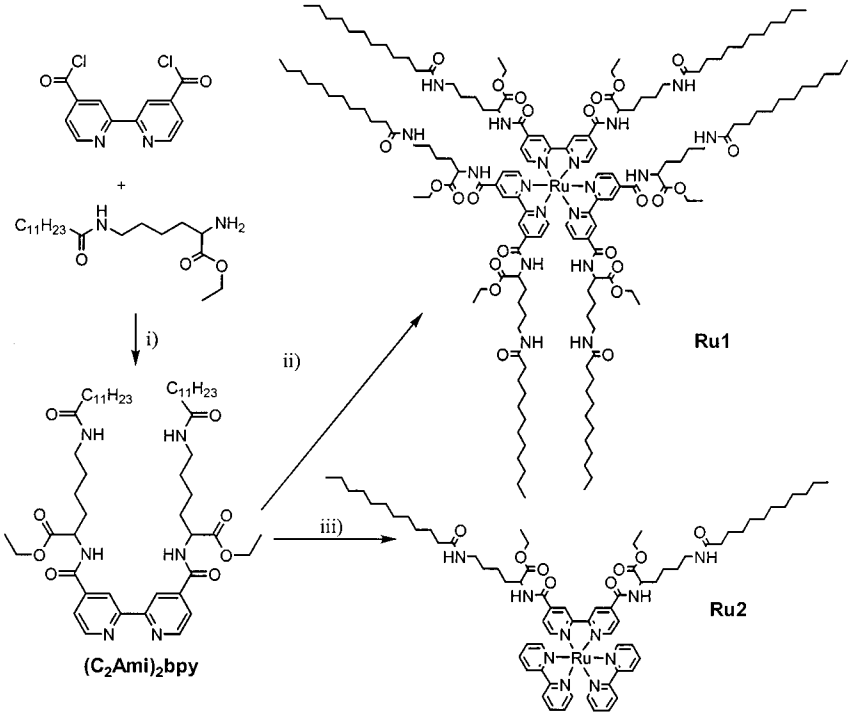

i) dry THF/dryNEt$_3$; ii)RuCl$_3$ 3H$_2$O/EtOH; iii)Ru(bpy)$_2$Cl$_2$ 2H$_2$O/80%EtOH

were recorded on a JASCO FS-420 spectrometer. UV−Vis absorption spectra were acquired on a Hewlett-Packard HP8452A diode array spectrometer or a JASCO V-570 UV/VIS/NIR spectrophotometer. Luminescence spectra were measured using a JASCO FP-750 spectrofluorimeter.

Gelation Test. In a typical gelation test, a weighed amount of **Ru1** or **Ru2** and 1 mL of solvent were combined in a glass test tube (1 cm diameter), which was sealed and then heated until complete dissolution was observed. The solution was allowed to cool to room temperature. Gelation was judged to have occurred when a homogeneous solution was obtained which did not flow when the test tube was tilted or inverted.

Transmssion Electron Microscopy (TEM). TEM images were obtained with a JEOL JEM-2010 electron microscope at 100 kV. Samples were prepared as follows: the compounds were dissolved in toluene or toluene−methanol and a drop of the solution was put on a collodion and carbon-coated 400 mesh copper grid. The grids were stored in a desiccator for 6 h, and then stored under reduced pressure overnight.

Steady-State Photolysis. Steady-state photolysis studies were conducted using the same apparatus described previously.[14] The reactions were carried out in methanol-toluene containing 1.1 $\times$ 10^{-5} M Ru complex and 1.0 $\times$ 10^{-3} M methyl viologen under an argon atmosphere at ambient temperature (22−24°). A spectroscopic cell (0.2 cm path length) was irradiated using a 300 W Xe lamp (ORIEL 500 W Xe and Hg/Xe arc lamp supply model 68811, ORIEL Co.) equipped with a UV cutoff filter (λ > 440 nm). Prior to the photolysis experiments, oxygen was expelled by bubbling argon gas into the sample solution for 15 min. The formation of the viologen radical calculated from the absorbance of the solution at 606 nm, corresponding to the maximum wavelength of the viologen radical (ϵ_{605} = 13400 mol^{-1} dm^3 cm^{-1}), and was monitored as a function of irradiation time. The initial rates of the viologen radical formation were calculated from the initial slope of a plot of the concentration of the viologen radical versus irradiation time. In all systems, the experimental errors were within ± 0.5%.

Nanosecond Flash Photolysis/Transient Diffuse Reflectance. Transient absorbance and emission measurements were carried out as described in detail elsewhere.[15] A 150 W Xe arc lamp was focused through a shutter window and 340 nm long pass filter onto the face of the cuvette at 45°. Approximately normal to the Xe light source, a 532 nm, 15 ns pulsed laser (Spectra Physics GCR-13 Nd:YAG, ca. 200 mJ/pulse) illuminated the same area of the cuvette.

Results and Discussion

Amphiphilic L-lysine derivatives are known for their gel-forming properties in organic solvents. The 2,2′-bipyridine ligand containing an L-lysine derivative at the 4,4′-positions [(C$_2$Ami)$_2$bpy] and ruthenium(II) complexes (**Ru1** and **Ru2**) were prepared according to Scheme 1. The synthesis of these Ru complexes follows easily from the (C$_2$Ami)$_2$bpy ligand, and in principle can be adapted to make gel-forming derivatives of a variety of transition metal polypyridyl complexes.

Ru2, which contains a single (C$_2$Ami)$_2$bpy ligand, has the ability to gel some aromatic solvents such as benzene, chlorobenzene, nitrobenzene, and chlorobenzene. In the same media, **Ru1**, which contains three (C$_2$Ami)$_2$bpy ligands, forms isotropic solutions. The minimum concentration for gelation of **Ru2** is 2 mg/mL in benzene and 4 mg/mL in toluene. Figure 1 shows TEM images of **Ru1** and **Ru2** prepared from toluene. Although both **Ru1** and **Ru2** form fiber structures, **Ru2** creates the network by entanglement of fine fibers. This hierarchical network structure is responsible for the gelation of **Ru2**. In contrast, **Ru1** forms a helical structure,[16] but not a network gel.

FTIR spectra were helpful in understanding the self-assembly of **Ru1** and **Ru2**. Spectra in chloroform, in which no self-assembly occurs, show absorption bands at 3440 and 1665 cm^{-1}, which are characteristic N−H and C═O stretching frequencies for non-hydrogen bonded amide groups. In contrast, spectra in toluene are very similar to those obtained for the complexes in the solid state. Both contain a band at 3320 cm^{-1}, which is

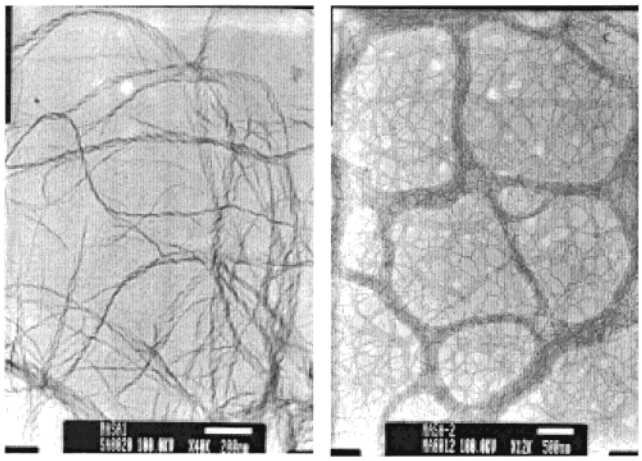

Figure 1. TEM images of **Ru1** (left) and **Ru2** (right) prepared from toluene. Scale bars are 200 and 500 nm, respectively.

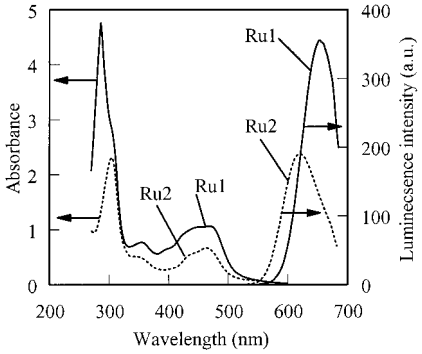

Figure 2. UV-vis absorption and luminescence spectra of **Ru1** (solid line) and **Ru2** (dotted line) in methanol−toluene (1:1, v/v). [**Ru1**] = 4.1×10^{-5} M and [**Ru2**] = 3.8×10^{-5} M.

TABLE 1: Photochemical and Photophysical Properties of a Series of Ru(II) Complexes

compd	$\lambda_{max,abs}$[a] (ϵ)	$\lambda_{max,em}$[b]	$\tau/\mu s$[c]
Ru1	466 (22 000)[d]	655	1.42
Ru2	468 (17 000)[d]	622	0.98
$Ru(bpy)_3^{2+}$	452 (14 500)[d]	611	0.85

[a] Absorption maxima (nm). [b] Luminescence maxima (nm). [c] Excited-state lifetimes at luminescence maxima obtained by laser flash photolysis.

assigned to the N−H vibration of hydrogen bonded amide groups. This indicates that hydrogen bonding contributes to the driving force for self-assembly. For **Ru2**, fine nanofibers are entangled in a complex way, probably through van der Waals interactions between terminal alkyl groups, and the network structure that leads to gelation is created.

By analogy to the well studied sensitizer $Ru(bpy)_3^{2+}$, the visible electronic transitions of **Ru1** and **Ru2** can be attributed to metal-to-ligand charge-transfer (MLCT), and emission occurs from the predominantly triplet MLCT excited state. Figure 2 shows absorption and emission spectra of **Ru1** and **Ru2** under conditions where both complexes exist in the solution state. Spectroscopic data for **Ru1** and **Ru2** are compared in Table 1 to those of $Ru(bpy)_3^{2+}$ in the same solvent system. The MLCT bands of **Ru1** and **Ru2** are red-shifted relative to $Ru(bpy)_3^{2+}$ and the extinction coefficients are larger; in particular, that of **Ru1** is almost double that of $Ru(bpy)_3^{2+}$. Both **Ru1** and **Ru2** have red-shifted luminescence and longer MLCT excited-state lifetimes than $Ru(bpy)_3^{2+}$. These differences are significantly larger for **Ru1** than for **Ru2**. Because **Ru1** has many hydrogen bonding sites, we postulate that it is more strongly interacting than **Ru2** in the self-assembling fibers. The thermal motion between Ru(II) and ligands is therefore more restricted in the case of **Ru1**, and this leads to a higher luminescence intensity and longer MLCT excited-state lifetime.

TABLE 2: Kinetic Parameters Obtained from Steady-state and Laser Flash Photolysis

	rate[a] [$\mu M\ s^{-1}$]	$k_q/10^8$ [$M^{-1}s^{-1}$]	ϕ_q[b]	$k_b/10^{10}$ [c] [$M^{-1}s^{-1}$]	$k_s/10^7$ [d] [$M^{-1}s^{-1}$]	$k_0/10^4$ [e] [s^{-1}]
Ru1	24.1	1.54	0.18	0.69	4.35	2.2
Ru2	9.8	1.83	0.15	1.16	2.82	2.4
$Ru(bpy)_3^{2+}$	5.1	5.52	0.32	4.96	1.67	12.0

[a] Initial rate of $MV^{+\bullet}$ formation at [Ru(II)] = 1.1×10^{-5} M, [MV^{2+}] = 1.0×10^{-3} M, and [TEOA] = 0.1 M. [b] Quantum yield for electron-transfer quenching of the MLCT excited state, from eq 4, using τ (= $1/k_r$) values from Table 1. [c] Rate constants for back electron transfer obtained from $MV^{+\bullet}$ decay curves at [Ru(II)] = 1.1×10^{-5} M and [MV^{2+}] = 3.0×10^{-3} M. [d] Rate constant for reduction of Ru(III) by TEOA, from bleaching recovery of the Ru(II) transient absorbance. [e] Average k_0 value, as defined in eq 12, for each sensitizer obtained by fitting steady-state photolysis data at [Ru(II)] = 1.1×10^{-5} M, [MV^{2+}] = 1.0×10^{-3} M.

Scheme 2[a]

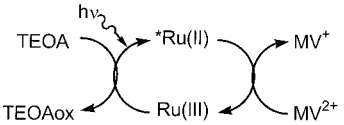

[a] (i) dry THF/dry NEt_3; (ii) $RuCL_3$ $3H_2O$/EtOH; (iii) $Ru(bpy)_2Cl_2$ $2H_2O$/80% EtOH.

Under an argon atmosphere, methyl viologen radical ($MV^{+\bullet}$) was formed by visible light irradiation (λ > 440 nm) of methanol-toluene solutions containing Ru(II) photosensitizers, methyl viologen (MV^{2+}), and triethanolamine (TEOA). The concentrations of sensitizers (1.1×10^{-5} M in methanol-toluene) was kept well below the gel transition in these experiments. Interestingly, with the self-assembling Ru(II) photosensitizers, the initial rate of $MV^{+\bullet}$ formation was higher; in particular, the initial rate with **Ru1** was about five times as high as that with $Ru(bpy)_3^{2+}$ (Table 2). Because this enhancement in photoreduction yield is larger than can be accounted for by the longer MLCT lifetime of **Ru1**, we conducted a kinetic analysis to determine whether the increased rate was a consequence of supramolecular organization.

To consider the reaction mechanism in more detail, the rate constants for the elementary reactions were measured using laser flash photolysis. In these systems, the charge separation reaction proceeds according to Scheme 2 and its initial rate depends on the quenching (forward) reaction, the rate of back electron transfer from $MV^{+\bullet}$ to Ru(III), and the rate of reduction of Ru(III) to Ru(II) by TEOA. Dynamic Stern−Volmer plots for quenching of the MLCT excited state by methyl viologen, Figure 3, were linear for **Ru1**, **Ru2**, and $Ru(bpy)_3^{2+}$. As shown in Table 2, the rate constant for quenching of the excited state (k_q) was highest for $Ru(bpy)_3^{2+}$. Interestingly, **Ru1**, which has the highest rate of $MV^{+\bullet}$ formation under steady-state photolysis conditions, has the smallest value of k_q.

Table 2 gives rate constants derived from transient absorbance changes at 605 nm, where $MV^{+\bullet}$ absorbs strongly, following laser excitation of **Ru1**, **Ru2**, and $Ru(bpy)_3^{2+}$ containing methanol-toluene solutions. The $MV^{+\bullet}$ decay at 605 nm obeys second-order kinetics and the second-order rate constants (k_b) are in the order of **Ru1** < **Ru2** < $Ru(bpy)_3^{2+}$: that is, the lifetime of $MV^{+\bullet}$ in the self-assembling Ru(II) complex systems is substantially longer than that in the $Ru(bpy)_3^{2+}$ system.

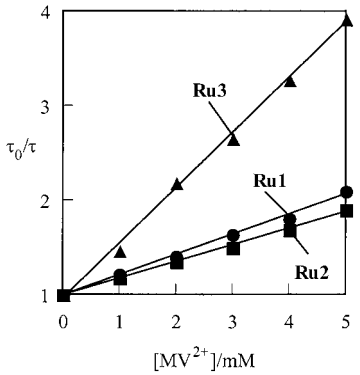

Figure 3. Stern−Volmer plots for luminescence quenching of **Ru1** (**J**), **Ru2** (**B**), and $Ru(bpy)_3^{2+}$ (H) by MV^{2+} in methanol−toluene.

Moreover, the second-order rate constant for reduction of Ru(III) to Ru(II) by TEOA (k_s), determined by measuring the Ru(II) bleaching recovery rate at different TEOA concentrations, are in the order of **Ru1** > **Ru2** > $Ru(bpy)_3^{2+}$.

These results indicate that the more effective charge separation for the self-assembling photosensitizers is caused by a slow back reaction with $MV^{+\bullet}$ and fast scavenging of Ru(III), relative to the $Ru(bpy)_3^{2+}$ system. The TEOA molecules, which contain functional hydrogen bond donor and acceptor groups, are most likely concentrated around the Ru(II) complex-core by hydrogen bonding. The slower rate constants for quenching of the excited state, as well as the slower back reactions between $MV^{+\bullet}$ and Ru(III), are tentatively attributed to Coulombic repulsion between the self-assembling fibers and the cationic viologen ions. Similar slowing of forward and back electron-transfer rates has been observed with polyelectrolyte sensitizers and acceptors in aqueous systems.[17]

The rate constants measured by transient spectroscopy can be related quantitatively to the steady-state photolysis yields by considering the reaction mechanism in more detail. Steady-state irradiation produces the MLCT excited state at a constant rate, $k_{h\nu}$, according to reaction 1. The excited state decays by a combination of radiative and nonradiative pathways, one of which is quenching by MV^{2+} (2). The remainder can be grouped together into the first-order decay reaction 3, which is characterized by the rate constant k_r

$$[RuL_3]^{2+} \xrightarrow{k_{h\nu}} [RuL_3]^{2+*} \tag{1}$$

$$[RuL_3]^{2+*} + MV^{2+} \xrightarrow{k_q} \{[RuL_3]^{3+} \text{- - -} MV^{+\bullet}\} \tag{2}$$

$$[RuL_3]^{2+*} \xrightarrow{k_r} [RuL_3]^{2+} \tag{3}$$

The quenching yield ϕ_q may be calculated from k_q and k_r according to (4). Once formed, the caged $\{[RuL_3]^{3+} \text{- - -} MV^{+\bullet}\}$-complex can separate by reaction 5 or undergo back electron

$$\phi_q = \frac{k_q[MV^{2+}]}{k_q[MV^{2+}] + k_r} \tag{4}$$

transfer 6 to regenerate the reactants. The cage escape

$$\{[RuL_3]^{3+} \text{- - -} MV^{+\bullet}\} \xrightarrow{k_{ce}} [RuL_3]^{3+} + MV^{+\bullet} \tag{5}$$

$$\{[RuL_3]^{3+} \text{- - -} MV^{+\bullet}\} \xrightarrow{k_{cr}} [RuL_3]^{2+} + MV^{2+} \tag{6}$$

yield ϕ_{ce} is derived from k_{ce} and k_{cr} according to 7

$$\phi_{ce} = \frac{k_{ce}}{k_{ce} + k_{cr}} \tag{7}$$

Once formed by reaction 5, Ru (III) can be reduced to Ru (II) by reaction with TEOA or $MV^{+\bullet}$ according to eqs 8 or 9, respectively. Again, from the branching of these two

$$[RuL_3]^{3+} + TEOA \xrightarrow{k_s} [RuL_3]^{2+} + \text{decomposition products} \tag{8}$$

$$[RuL_3]^{3+} + MV^{+\bullet} \xrightarrow{k_b} [RuL_3]^{2+} + MV^{2+} \tag{9}$$

kinetic pathways, the quantum yield for reduction of Ru(III) by TEOA may be calculated eq 10

$$\phi_s = \frac{k_s[TEOA]}{k_s[TEOA] + k_b[MV^{+\bullet}]} \tag{10}$$

By combining these quantum yields with the generation rate $k_{h\nu}$, we obtain a differential eq 11 that describes the rate of formation of $MV^{+\bullet}$

$$\frac{d[MV^{+\bullet}]}{dt} = k_{h\nu}\phi_q\phi_{ce}\phi_s = k_0\frac{k_s[TEOA]}{k_s[TEOA] + k_b[MV^{+\bullet}]} \tag{11}$$

In which k_0 is defined as

$$k_0 \equiv k_{h\nu}\phi_q\phi_{ce} \tag{12}$$

Solving this equation gives the integrated rate law 13

$$[MV^{+\bullet}] = \frac{k_0k_s[TEOA]}{k_b}\left\{-\frac{1}{k_0} + \left[\left(\frac{1}{k_0}\right)^2 + \frac{2k_bt}{k_0k_s[TEOA]}\right]^{1/2}\right\} \tag{13}$$

which predicts a linear growth in $MV^{+\bullet}$ concentration at early times in the reaction, followed by an approximately $t^{1/2}$ growth at later times.

Figure 4 shows steady-state photolysis data, along with the behavior expected from eq 13. Individual k_0 values were obtained by one-parameter fitting of photolysis data acquired over a range (0.1 to 1.0 M) of TEOA concentrations. In each case the fit was constrained by the k_s/k_b ratio (Table 2) measured by transient spectroscopy. The lines shown in Figure 4, which use the average of the k_0 values obtained for each sensitizer (Table 2), fit the data only approximately. This is especially true at longer times where background processes (such as reaction of $MV^{+\bullet}$ with water and oxygen) cause some flattening of the expected $t^{1/2}$ behavior.

A number of factors could contribute to the observed systematic departure from the simple (homogeneous) kinetic model proposed above. Although the MLCT decays are single-exponential for **Ru1** and **Ru2** (implying that the micro-environment is similar for all sensitizer molecules), the distribution of MV^{2+} and TEOA in the nanofibers is not necessarily homogeneous. Diffusion of molecules in these organized media is most likely not a stochastic process. Other factors, such as background oxidation or decomposition of viologen radicals, could also contribute to flattening of the photolysis curves. Nevertheless, the general shape of all the curves, including those not shown, is roughly that expected from the kinetic model, and so conclusions can be drawn from the major trends. We note that the ordering of k_0 values derived for **Ru1**, **Ru2**, and $Ru(bpy)_3^{2+}$ follows the trend in ϕ_q, as expected from eq 12. By

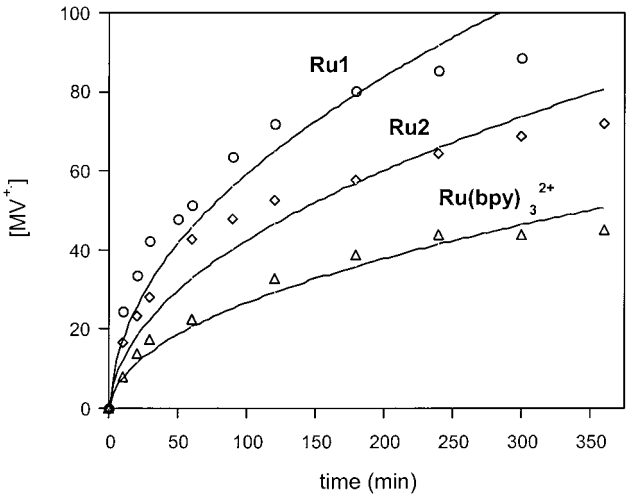

Figure 4. Steady state photolysis plot for **Ru1**, **Ru2**, and $Ru(bpy)_3^{2+}$ at [Ru(II)] = 1.1×10^{-5} M, [MV^{2+}] = 1.0×10^{-3} M, and [TEOA] = 0.1 M. Solid lines show the behavior predicted from eq 13, using k_s and k_b values from Table 2. The k_0 values used to plot the lines are averages obtained from single parameter fits to eq 13, obtained over a range of TEOA concentrations.

comparing k_0 values, we can also conclude that the cage escape yields, ϕ_{ce}, are significantly lower for **Ru1** and **Ru2** than they are for $Ru(bpy)_3^{2+}$.

Conclusions

We have found that Ru(II) complex photosensitizers containing L-lysine side chains form fibrous supramolecular structures. Despite their lower quenching rates and cage escape yields, the photolysis reaction is more efficient with **Ru1** and **Ru2** than it is with $Ru(bpy)_3^{2+}$. The improvement derives from the much slower back electron-transfer rates, k_b, and the enhanced rates of the donor reaction, k_s, for the supramolecular sensitizers. These effects are most pronounced for **Ru1**, which contains six L-leucine containing side chains, than they are for **Ru2**, which contains only two such side chains.

Laser flash photolysis measurements confirm that the lifetime of $MV^{+\bullet}$ in these systems is long and that the reduction of the Ru(III) to Ru(II) is fast compared to the simple $Ru(bpy)_3^{2+}$ system. These results are encouraging for the design of other donor-sensitizer-acceptor systems, because they demonstrate that hydrogen bonding and Coulombic effects in supramolecular aggregates of sensitizers can be used effectively to enhance photoproduct yields.

Acknowledgment. This work was supported by the Division of Chemical Sciences, Office of Basic Energy Sciences, Department of Energy, under Contract No. DE-FG02-93-ER14374 and Grant-in-Aid for COE research (10CE2003) from the Ministry of Education, Culture, Science, Sports, and Technology of Japan.

References and Notes

(1) (a) Lehn, J.-M. *Science* **1993**, *260*, 1762−1763. (b) Lehn, J.-M. *Supramolecular Chemistry: Concepts and Perspectives*; VCH: Weinheim, Germany, 1995.

(2) (a) Constable, E. C.; Smith, D. *Chem. Br*. **1995**, *1*, 33−37, 41. (b) Lindsey, J. S.; *New J. Chem*. **1991**, *15*, 153−180. (b) Lawrence, D. S.; Jiang, T.; Levett, M. *Chem. Rev*. **1995**, *95*, 2229−2260. (c) Lehn, J.-M. In *Perspectives in Coordination Chemistry*; Williams, A. F., Floriani, C., Merbach, A. E., Eds.; Verlag: *Helvetica Chimica Acta*: Basel, 1992; 447−462. (d) Sabbatini, N.; Guardigli, M.; Lehn, J.-M. *Coord. Chem. Rev*. **1993**, *123*, 201−228.

(3) For recent reviews see: (a) Philip, D.; Stoddart, J. F. *Angew. Chem., Int. Ed. Engl*. **1996**, *35*, 1154−1196. (b) Terech, P.; Weiss, R. G. *Chem. Rev*. **1997**, *97*, 3133−3159. (c) Terech, P. *Ber. Bunsen-Ges. Phys. Chem*. **1998**, *102*, 1630−1643. (d) van Esch, J. H.; Feringa, B. L. *Angew. Chem., Int. Ed*. **2000**, *39*, 2263−2266. (e) Abdallah, D. J.; Weiss, R. G. *Adv. Mater*. **2000**, *12*, 1237−1247.

(4) (a) Lin, Y.-C.; Kacher, B.; Weiss, R. G. *J. Am. Chem. Soc*. **1989**, *111*, 5542. (b) Lu, L.; Mattew Cocker, T.; Bachman, R. E.; Weiss, R. G. *Langmuir* **2000**, *16*, 20−34. (c) Abdallah, D. J.; Weiss, R. G. *Langmuir* **2000**, *16*, 352−355.

(5) (a) Murata, K.; Aoki, M.; Suzuki, T.; Harada, T.; Kawataba, H.; Komori, T.; Ohseto, F.; Ueda, K.; Shinkai, S. *J. Am. Chem. Soc*. **1994**, *116*, 6664. (b) Yoza, K.; Amonokura, N.; Ono, Y.; Aoki, T.; Shinmori, H.; Takeuchi, M.; Shinkai, S.; Reinhoudt, D. N. *Chem. Eur. J*. **1999**, *5*, 2722−2729. (c) Hafkamp, R. J. H.; Feiters, M. C.; Nolte, R. J. M. *J. Org. Chem*. **1999**, *64*, 412−426. (d) Hanabusa, K.; Yamada, M.; Kimura, M.; Shirai, H. *Angew. Chem., Int. Ed. Engl*. **1996**, *35*, 1949. (e) Hanabusa, K.; Tanaka, R.; Suzuki, M.; Kimura, M.; Shirai, H. *Adv. Mater*. **1997**, *9*, 1095. (f) Hanabusa, K.; Matsumoto, M.; Kimura, M.; Kakehi, A.; Shirai, H. *J. Colloid Interface Sci*. **2000**, *224*, 231−244.

(6) (a) Gu, W.; Lu, L.; Chapman, G. B.; Weiss, R. G. *Chem. Commun*. **1997**, 543−544. (b) Hafkamp, R. J. H.; Kokke, B. P. A.; Danke, I. M.; Geurts, H. P. M.; Rowan, A. E.; Feiters, M. C.; Nolte, R. J. M. *Chem. Commun*. **1997**, 545−546.

(7) (a) Kobayashi, S.; Hanabusa, K.; Hamasaki, N.; Kimura, M.; Shirai, H.; Shinkai, S. *Chem. Mater*. **2000**, *12*, 1523−1525. (b) Jung, J. H.; Ono, Y.; Shinkai, S. *Angew. Chem., Int. Ed*. **2000**, *39*, 1862−1865. (c) Jung, J. H.; Ono, Y.; Hanabusa, K.; Shinkai, S. *J. Am. Chem. Soc*. **2000**, *122*, 5008−5009.

(8) (a) Li, S.; John, V. T.; Irvin, G. C.; Bachakonda, S. H.; Mcpherson, G. L.; O'Connor, C. J. *J. Appl. Phys*. **1999**, *85*, 5965−5967. (b) Velasco-García, N.; Valencia-Gonzáez, M. J.; Díaz-García, M. E. *Analyst* **1997**, *122*, 1405−1409.

(9) (a) Inoue, K.; Ono, Y.; Kanejo, Y.; Ishi-i, T.; Yoshihara, K.; Shinkai, S. *J. Org. Chem*. **1999**, *64*, 2933−2937. (b) Shinkai, S.; Murata, K. *J. Mater. Chem*. **1998**, *8*, 485−495.

(10) (a) Hanabusa, K.; Hiratsuka, K.; Kimura, M.; Shirai, H. *Chem. Mater*. **1999**, *11*, 649−656. (b) Mizoshita, N.; Kutsuna, T.; Hanabusa, K.; Kato, T. *J. Photopolym. Sci. Technol*. **2000**, *13*, 307−313.

(11) Hanabusa, K.; Nakayama, H.; Kimura, M.; Shirai, H. *Chem. Lett*. **2000**, *9*, 1070−1071.

(12) Suzuki, M.; Waraksa, C. C.; Nakayama, H.; Hanabusa, K.; Kimura, M.; Shirai, H. *Chem. Commun*. **2001**, 2012−3.

(13) Garelli, N.; Vierling, P. *J. Org. Chem*. **1992**, *57*, 3046−3051.

(14) Hara, M.; Waraksa, C. C.; Lean, J. T.; Lewis, B. A.; Mallouk, T. E. *J. Phys. Chem. A* **2000**, *104*, 5275.

(15) Saupe, G. B.; Kim, W.; Schmehl, R. H.; Mallouk, T. E. *J. Phys. Chem. B* **1997**, *101*, 2491.

(16) Suzuki, M.; Nakayama, H.; Hanabusa, K.; Kimura, M.; Shirai, H., manuscript in preparation.

(17) (a) Sassoon, R. E.; Gershuni, S.; Rabani, J. *J. Phys. Chem*. **1992**, *96*, 4692. (b) Rabani, J. in *Photoinduced Electron Transfer*; Fox, M. A., Chanon, M., Eds.; Elsevier: Amsterdam, 1988; Part B, pp 642−696. (c) Sassoon, R. E. *J. Am. Chem. Soc*. **1985**, *107*, 6133. (d) Rabani, J.; Sassoon, R. E. *J. Photochem*. **1985**, *29*, 7. (e) Morishima, Y.; Itoh, Y.; Nozakura, S.-I.; Ohno, T.; Kato, S. *Macromolecules* **1984**, *17*, 2264.